

Ion Exchange Lithography: Localized Ion Exchange Reactions for Spatial Patterning of Perovskite Semiconductors and Insulators

Lukas Helmbrecht, Moritz H. Futscher, Loreta A. Muscarella, Bruno Ehrler, and Willem L. Noorduin*

Patterning materials with different properties in a single film is a fundamental challenge and essential for the development of next-generation (opto)electronic functional components. This work introduces the concept of ion exchange lithography and demonstrates spatially controlled patterning of electrically insulating films and semiconductors with tunable optoelectronic properties. In ion exchange lithography, a reactive nanoparticle “canvas” is locally converted by printing ion exchange “inks.” To demonstrate the proof of principle, a canvas of insulating nanoporous lead carbonate is spatioselectively converted into semiconducting lead halide perovskites by contact printing an ion exchange precursor ink of methylammonium and formamidinium halides. By selecting the composition of the ink, the photoluminescence wavelength of the perovskite semiconductors is tunable over the entire visible spectrum. A broad palette of conversion inks can be applied on the reactive film by printing with customizable stamp designs, spray-painting with stencils, and painting with a brush to inscribe well-defined patterns with tunable optoelectronic properties in the same canvas. Moreover, the optoelectronic properties of the converted canvas are exploited to fabricate a green light-emitting diode (LED), demonstrating the functionality potential of ion exchange lithography.

Spatial arrangement of materials with contrasting properties is fundamentally interesting and essential for integrated (opto)electronic devices.^[1,2] Nanoparticles are versatile building blocks for achieving such arrangement by both bottom-up and top-down assembly.^[2–22] Spatial patterning of nanoparticles has been achieved by methods such as patchy particles, oriented

attachment, hierarchical self-assembly, topological templates, and optical and e-beam lithography.^[2–16,23] Moreover, the entire ensemble of nanoparticles can be converted into a desirable chemical composition using ion exchange reactions, while preserving the pattern of the ensemble.^[4,17–22] Also, selected areas of the ensemble can first be encapsulated with a passivating coating, after which only the uncoated nanoparticles undergo conversion during ion exchange.^[24] Hence, organization of different composition is possible in many ways, but often requires multiple steps to achieve control over patterning and chemical composition, making the overall process difficult and expensive.^[2,16]

Locally applying the reagents offers an alternative approach for spatial arrangement of materials with desirable properties. For thousands of years, printing of inks on canvases has spurred human development. Recently, methods such as microcontact printing have been used


extensively to locally functionalize substrates and infuse reactants in gels.^[25–28] Inspired by these works, we here introduce the concept of ion exchange lithography (IEL). We show that spatial patterning of materials can simply be achieved by printing ion exchange “inks” on a reactive nanoparticle “canvas.” Importantly, to act as a versatile canvas, the nanoparticle film should enable ion exchange to many different chemical compositions. The ink, on the other hand, should react the contacted area of the canvas to one specific composition only, while other reaction products ideally leave the canvas automatically.

To demonstrate the proof-of-principle of IEL, we explore the spatially controlled conversion of an electrically insulating canvas into semiconducting lead halide perovskites. The extraordinary properties of perovskites, in combination with their simple synthesis, is revolutionizing the field of optoelectronics.^[29–31] Spatially organizing perovskites alongside materials with fundamentally different properties is essential for integrated devices such as displays, detectors, and scintillators.^[32–37] Spatial positioning of perovskites has been achieved using, for instance, photolithography, laser writing, templates, nanoimprint lithography, and inkjet printing.^[38–47] and post synthesis modification of perovskites has enabled local modification of the light emission color.^[48,49] Nevertheless, such approaches are often laborious

Dr. L. Helmbrecht, Dr. M. H. Futscher, L. A. Muscarella, Prof. B. Ehrler, Prof. W. L. Noorduin
AMOLF

Science Park 104, Amsterdam 1098 XG, The Netherlands
E-mail: noorduin@amolf.nl

Prof. W. L. Noorduin
Van 't Hoff Institute for Molecular Sciences
University of Amsterdam
Science Park 904, Amsterdam 1090 GD, The Netherlands

 The ORCID identification number(s) for the author(s) of this article can be found under <https://doi.org/10.1002/adma.202005291>.

© 2021 The Authors. Advanced Materials published by Wiley-VCH GmbH. This is an open access article under the terms of the Creative Commons Attribution License, which permits use, distribution and reproduction in any medium, provided the original work is properly cited.

DOI: 10.1002/adma.202005291

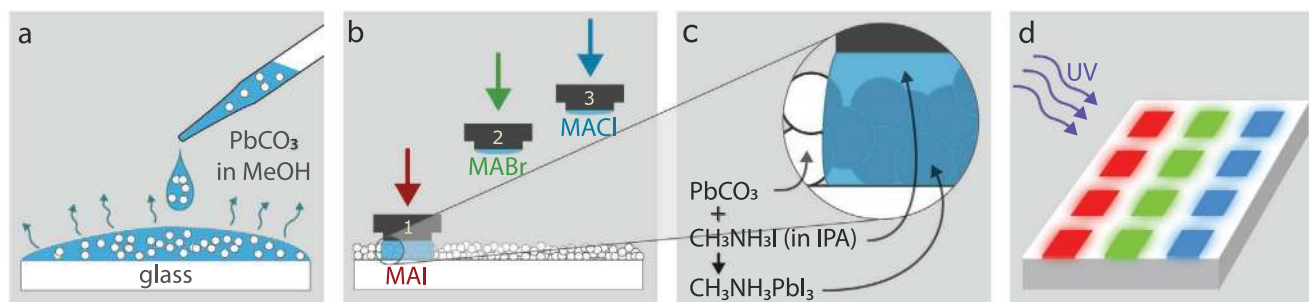
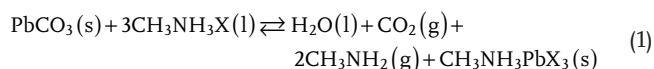


Figure 1. Schematic illustration showing the fabrication of a spatially patterned perovskite film. a) Drop casting PbCO_3 particles dispersed in methanol onto a glass substrate results in a PbCO_3 thin film that acts as the reactive canvas. b) Stamping MAX in IPA on the canvas results in, c) spatially-controlled conversion of the PbCO_3 into a MAPbX_3 perovskite. d) Upon UV irradiation, the converted areas emit light with a color that is controlled by adjusting the halide moiety of the perovskite.

and slow, and require specialized equipment, thus making them difficult to scale up. This highlights the need for new strategies to directly achieve spatial organization of desirable compositions in a simple and scalable manner.

Here we integrate semiconducting perovskites in an electrically insulating film by printing, painting, and spraying reactive inks on an ion exchange reactive canvas. Note that while the previously developed techniques achieve patterns through depositing, removing, or shaping perovskite, we here convert an insulating film into perovskite. The versatility of this IEL approach allows for scalability and arbitrary, user-defined patterns. The photoluminescence wavelength of the perovskite semiconductors is tunable over the entire visible spectrum by selecting the composition of the ink. Moreover, we show that the IEL approach can be integrated into the fabrication of (opto) electronic devices such as light-emitting diodes (LED).

Our approach is illustrated in **Figure 1**. In short, nanoscopic lead carbonate (PbCO_3) crystals are deposited in a thin film. This electronically insulating PbCO_3 film acts as reactive canvas, while a solution of methylammonium halides ($\text{CH}_3\text{NH}_3\text{X}$ or MAX; X = Cl, Br, or I) is the reactive ink. Contact printing of the ink on the canvas results in the local conversion of PbCO_3 into semiconducting methylammonium lead halide perovskites ($\text{CH}_3\text{NH}_3\text{PbX}_3$ or MAPbX_3 ; X = Cl, Br, or I) following the previously developed reaction:^[21]



The acidic pH facilitates the replacement of carbonate for the halide anion, followed by insertion of the methylammonium halide to rearrange the crystal structure into the perovskite. This reaction is ideal for testing our approach: the PbCO_3 is insoluble and thus suitable for acting as the reactive canvas, while $\text{CH}_3\text{NH}_3\text{X}$ can be dissolved in common solvents such as isopropyl alcohol (IPA) and therefore act as the ink.^[50] Moreover, the PbCO_3 canvas can react into perovskites with different chemical compositions, where the choice of the $\text{CH}_3\text{NH}_3\text{X}$ ink will determine the exact composition of the perovskite that forms in the canvas. The solvent, as well as the other reaction products, water (H_2O), carbon dioxide (CO_2), and methylamine (CH_3NH_2) simply evaporate from the film, thus driving the reaction from PbCO_3 to perovskite.

To demonstrate the proof-of-principle, we fabricate nanoporous films by drop casting nanoscopic PbCO_3 crystals onto glass substrates (see Supporting Information for details). High-resolution scanning electron microscopy (SEM) shows that the particles have typical sizes between 40 and 300 nm, and are densely packed into uniform films while still exhibiting nanoscale porosity (**Figure 2a**). We find that the film thickness can be tuned between ≈ 0.25 – $5.0 \mu\text{m}$ by controlling the drop casting conditions (Figure 2 and Supporting Information).

We perform the ion exchange contact printing by bringing the PbCO_3 film in contact with a solution of MAX in anhydrous isopropyl alcohol (IPA). IPA was selected as solvent based on the following criteria: 1) The solvent should dissolve the precursors MAX, while 2) not dissolving the perovskite (hence disqualifying solvents such as DMSO and DMF). 3) The vapor pressure should be sufficiently high to enable full evaporation. 4) The solvent should enable partial wetting of the film by capillary forces. The conversion ink is applied using customized silicone and poly(dimethylsiloxane) (PDMS) stamps (see Supporting Information). These materials are easily moldable and chemically inert. In addition, the hardness of these materials can be tuned to achieve uniform contact between the film and the stamp while keeping the canvas intact (see Supporting Information).^[25,27]

The local conversion is demonstrated by applying MABr-IPA on the PbCO_3 canvas using a stamp patterned with rectangular pillars. Within seconds the white PbCO_3 transforms into yellow-orange perovskite at the points of contact with the stamp, thereby meticulously replicating the pattern of the stamp with high fidelity (see Supporting Information for comparison of a stamp and stamped pattern). Moreover, infrared (IR) spectroscopy confirms the absence of side products on the converted film (see Supporting Information).

The optoelectronic properties of the converted pattern can directly be visualized by exciting the electronic structure with an ultraviolet (UV) light source (Figure 2d). We observe bright green photoluminescence (PL) from the converted rectangles, whereas the lead carbonate in the pristine part of the film did not convert to the perovskite and therefore did not emit any light. Photoluminescence spectroscopy showed that the emission wavelength of the converted pattern peaked at 530 nm, which is consistent with previous PL measurements of MAPbBr_3 .^[21]

We explore the scalability of the pattern dimensions. For most practical applications, feature sizes on the order of $100 \mu\text{m}$ are

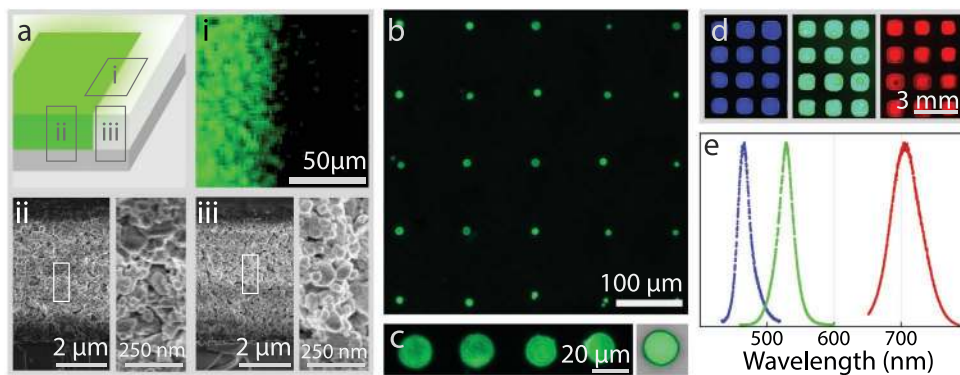


Figure 2. Characterization of contact printed perovskite pixels. a) Schematic overview of a printed pixel: i) EDS elemental mapping of Br atoms, ii) cross-section of a converted film with close-up (SEM), iii) cross-section of a pristine film with close-up (SEM). b) Photoluminescence microscopy image of a square array of contact printed dots spaced 100 μm apart. c) Photoluminescence microscopy image of: (left) array of 20 μm dots spaced 40 μm , (right) 20 μm PDMS stamp overlaid with the resulting photoluminescence dot pattern. d) Fluorescence photographs of contact-printed perovskite pixels of different emission colors by tuning the halide moiety: left to right: MACl-MABr (6:4), MABr, MABr-MAI (2:8). e) Corresponding normalized photoluminescence spectra of the perovskites shown in Figure 2d.

required (e.g., 150 μm pixel size in a 13" full HD display). We use a high-resolution PDMS stamp with a height of 10 μm and a diameter of 20 μm pillars that are spaced 100 μm apart. Again, the pattern is faithfully replicated into an array of perovskite dots (Figure 2b). We investigate the resolution limits by comparing the stamp with the resulting pattern. Deliberate overwetting the stamp results in broadening of the pattern, suggesting lateral spreading within the film due to capillary forces. Optimizing the amount of applied ink allows minute replication of the PDMS stamp into a pattern with only slight size variations of 1–2 μm (Figure 2c). While capillary forces and ink volume currently limit the resolution, the ink is sufficiently wetting the film for the conversion reaction to occur while preserving the pattern.

The observed lateral spreading suggests that capillary forces will transport the ink also vertically into the depth of the film, thus enabling conversion throughout the canvas. Indeed, energy-dispersive X-ray spectroscopy (EDS) on a cross-sectioned sample reveals the presence of bromide throughout the depth of the canvas (Figure S3, Supporting Information). Combined with fluorescence photographs of the backside of the opaque canvas, this indicates conversion from the top to the bottom (see Figure S2, Supporting Information). In the lateral direction at the edge of the wetted area, a well-defined boundary between the converted and unconverted area is achieved, according to EDS (Figure 2a). Although the grains undergo conversion to perovskite, the nanoscopic morphology is conserved, as observed via high-resolution electron microscopy (Figure 2a). Moreover, films with only 3.5 at% bromide (as compared to lead) already show bright emission, although the conversion can be increased to 25 at% by prolonging the reaction time, whereas SEM analysis confirmed that the morphology of the particles remains preserved (see Supporting Information).

Reaction scheme 1 suggests that perovskites with different halide moieties—and therefore different emission colors—can be synthesized in the PbCO_3 film by selecting the corresponding methylammonium halide precursor in the ink. Indeed, mixing MAI into the MABr/IPA conversion ink yielded mixed-halide perovskite patterns with red PL, while MACl addition resulted in blue PL (Figure 2d). The emission wavelength can be tuned

by the mixing ratios of different methylammonium halides in the conversion ink, for example, 6:4 molar ratio MACl:MABr/IPA resulting in bright emission around 465 nm (Figure 2e), whereas 8:2 molar ratio MAI:MABr yields deep red emission around 705 nm (Figure 2e). Hence, the color of the light-emitting patterns can be tuned over the whole visible spectrum.

IEL can be extended to other classes of perovskites. Formamidinium halide perovskites ($\text{CH}(\text{NH}_2)_2\text{PbX}_3$ or FAPbX_3) are of interest because of their greater chemical stability and longer carrier diffusion length while exhibiting comparable optical performance to methylammonium perovskites.^[51,52] Conversion of PbCO_3 to FAPbX_3 is achieved using formamidinium halides instead of methylammonium halides in the precursor ink. Akin to MAX (reaction scheme 1), formamidinium halide (FAX) can partly dissociate to form acid and thereby drive the exchange of carbonate with the halide group. Moreover, the chemical similarities between MAX and FAX as well as the structural similarities between the crystal lattices of MAPbX_3 and FAPbX_3 suggest an equivalent reaction pathway. The resulting FAPbX_3 perovskite patterns show bright luminescence with tunable PL emission throughout the visible spectrum by selecting the halide moiety between chloride, bromide, and iodide (Figure S4, Supporting Information).

Based on these insights, we integrate perovskites with different emission wavelengths into a single canvas. To this aim, we sequentially print the ion mixtures for different perovskites on the lead carbonate film. Accurate spatial positioning of the different stamps is achieved by a guiding framework (see Supporting Information). To demonstrate the principle, we integrate rectangles of red, green, and blue-emitting semiconductors within the non-luminescent insulator to produce an array pattern akin to the ones commonly used in LED displays (Figure 3a).

The ion exchange inks can be applied using many other traditional and scalable inking techniques such as inkjet-, offset-, and roll-to-roll printing. From this extensive repertoire, we test traditional artist's paintbrushes and an airbrush gun. With the paintbrush, freeform patterns can be achieved straightforwardly (Figure 3b). With the airbrush gun, large uniform areas can be converted. Moreover, highly complex patterns can be achieved using laser-cut stencils as a shadow

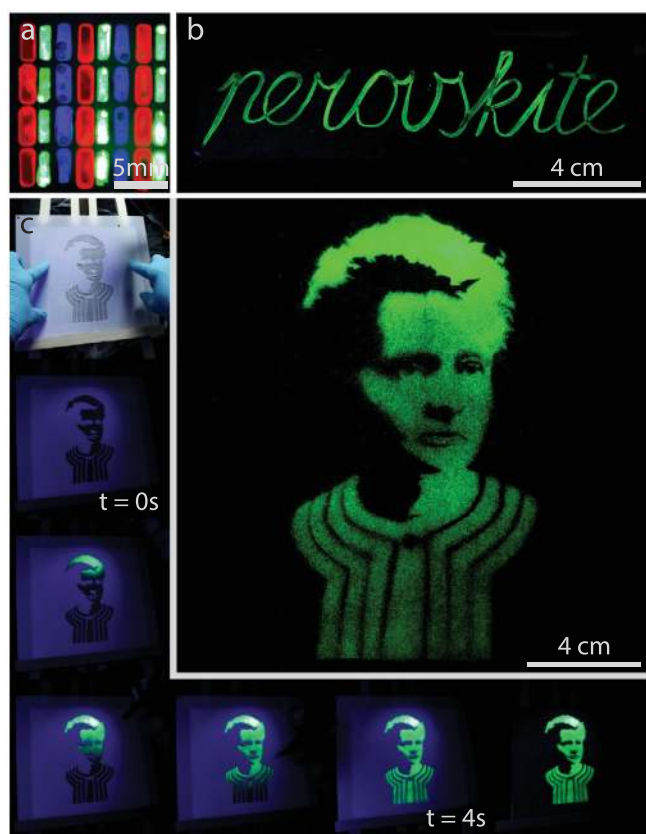


Figure 3. IEL via different printing techniques. a) Fluorescence photograph of multicolor contact printed pixels: FABr-FAI (2:8) (red), MABr (green), and MACI-MABr (6:4) (blue) separated by unconverted PbCO_3 . b) Fluorescence photograph of a pattern drawn by applying the conversion ink with a paintbrush. c) Time-lapse of an airbrush painting of Marie Skłodowska-Curie: a 20×20 cm film of PbCO_3 is selectively shielded with a stencil (the polymer in the stencil fluoresces blue under UV irradiation), MABr/IPA is applied with an airbrush gun, the ion exchange reaction creates perovskite that luminesces green under UV irradiation, removal of the stencil shows the portrait. The Marie Skłodowska-Curie image is reproduced under the terms of the CC-BY Creative Commons Attribution 4.0 International license (<http://creativecommons.org/licenses/by/4.0>).^[62] Copyright: Wellcome Collection.

mask, which we exploit for creating a green luminescent portrait of Marie Skłodowska-Curie. (Figure 3c; Movie S1, Supporting Information). An additional advantage of airbrushing is that this method is fast and contact-free while easily converting sizeable areas, hence averting the risk of damaging the film and offering compatibility for large-scale fabrication.

IEL offers exciting opportunities for the direct integration of materials with different electronic properties in functional devices. The converted MAPbBr_3 and FAPbBr_3 films show good photoluminescence quantum yields (PLQY) of $25 \pm 3\%$ and $40 \pm 5\%$ respectively, making them promising candidates for optoelectronic components. We explore this potential by fabricating an LED with FAPbBr_3 as the active layer (see Figure 4a,b and Supporting Information), and comparing this LED to a device based on a conventional spin coated FAPbBr_3 film with an identical layer stack. We characterize both devices by recording the current–voltage (I – V) curves as well as measuring

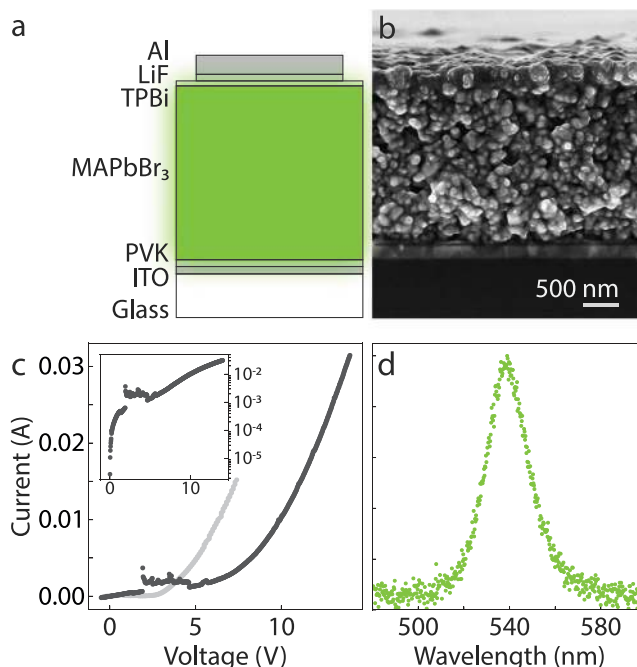


Figure 4. LED based on IEL. a) Schematic of the layers used in this LED, b) Cross section of a device imaged by SEM. c) I – V measurement of an IEL-based LED (black, inset logarithmic scale) and a conventional LED (gray), and d) normalized EL showing green light emission of the LED at 10 V.

electroluminescence (EL). As expected for FAPbBr_3 LEDs, the I – V curves display typical diode characteristics (Figure 4c). The ion-exchange-based device exhibits a higher turn-on voltage indicating an increased resistance, likely due to the partially insulating nanoparticle interior of the film. Nevertheless, with applied voltage, the device operates as a light-emitting diode (LED) and emits green EL around 540 nm as previously reported (Figure 4d).^[53,54] While the performance may be further optimized by improving the connectivity between the particles themselves as well as with the electrodes, this proof-of-concept device already demonstrates the potential of IEL for functional (opto)electronic devices.

In conclusion, we here demonstrate spatially controlled ion exchange reactions of lead carbonate films into lead halide perovskites. We show that this ion exchange-lithography method offers a simple, scalable, versatile, and highly customizable method for integrating desirable complementary electronic and optoelectronic properties in arbitrary patterns that can be integrated into functional devices. Effectively, the conversion liquid and film can be regarded as reactive ink and canvas for integrating unusual and attractive properties with micrometer spatial control.

Semiconductors and lead carbonates have a long history in painting and other arts. Basic lead carbonate is one of the oldest synthetic pigments known, while semiconducting salts such as cadmium sulfide and lead chromate enabled bright colors and were widely adopted by painters such as Monet and Van Gogh.^[55–58] Traditionally, artists apply the semiconductors as pigment on the canvas. In contrast, our work enables conversion of the canvas into a semiconductor by painting a reactive ink.

Currently, the resolution of the patterns is mainly determined by: 1) properties of the ink (e.g., viscosity, volatility, polarity,

wetting behavior), 2) the applied volume of ink, 3) properties of the film (e.g., porosity, particle size, surface chemistry, etc.), and 4) the thickness of the film. The capillary forces are determined by the combined properties of the ink and the film, and balancing their contributions enables optimization of the resolution. Since the resolution of the converted patterns is to a large extent defined by the precision with which the conversion ink is applied, state-of-the-art technologies such as roll-to-roll and inkjet printing can be exploited. Moreover, photoinduced ion exchange reactions may offer opportunities for further improving the resolution with spatially controlled light patterns.

Already, many ion exchange reactions have been developed in liquids.^[17–21] We therefore envisage that the palette of conversion inks for our IEL methodology can straightforwardly be extended to a wide range of chemical compositions with desirable and unusual properties. In addition, we foresee that nanocomposites could serve as attractive conversion canvases due to their outstanding mechanical properties and chemical reactivity.^[21,59–61] Consequently, IEL may offer an attractive route for the synthesis of functional integrated devices such as displays and detectors that require complicated spatial patterning of complementary properties in a single film. Therefore, exciting opportunities will arise from expanding the microelectronic paint box, adding conversion inks for the synthesis of other semiconductors, transport layers, and conductors, which ultimately enables fully printed devices with ion exchange lithography.

Supporting Information

Supporting Information is available from the Wiley Online Library or from the author.

Acknowledgements

The authors thank Dion Ursem for designing and fabricating the stamp and guiding system. The authors thank Christiaan van Campenhout for assistance in creating the portrait of Marie Skłodowska-Curie and Marloes H. Bistervels for help in creating the “perovskite” lettering in Figure 3b. The authors thank Jian-Yao Zheng for assistance with the PLQY measurements. The authors thank Christiaan van Campenhout and Alexander Korotkevich for their assistance with the FTIR measurements. This work was part of the Vernieuwingsimpuls Vidi research program “Shaping up materials” with project number 016.Vidi.189.083, which was partly financed by the Dutch Research Council (NWO). The work of L.A.M. was part of the Vidi research program 016.Vidi.179.005.

Conflict of Interest

The authors declare no conflict of interest.

Keywords

ion exchange, ion exchange lithography, perovskites

Received: August 4, 2020
Revised: December 8, 2020
Published online:

- [1] M. Faustini, L. Nicole, E. Ruiz-Hitzky, C. Sanchez, *Adv. Funct. Mater.* **2018**, *28*, 1704158.
- [2] J. H. Choi, H. Wang, S. J. Oh, T. Paik, P. S. Jo, J. Sung, X. Ye, T. Zhao, B. T. Diroll, C. B. Murray, C. R. Kagan, *Science* **2016**, *352*, 205.
- [3] M. G. Ma, H. Cölfen, *Curr. Opin. Colloid Interface Sci.* **2014**, *19*, 56.
- [4] M. P. Boneschanscher, W. H. Evers, J. J. Geuchies, T. Altantzis, B. Goris, F. T. Rabouw, S. A. P. P. Van Rossum, H. S. J. J. van der Zant, L. D. A. A. Siebbeles, G. van Tendeloo, I. Swart, J. Hilhorst, A. V. Petukhov, S. Bals, D. Vanmaekelbergh, *Science* **2014**, *344*, 1377.
- [5] J. J. de Yoreo, P. U. P. A. Gilbert, N. A. J. M. Sommerdijk, R. L. Penn, S. Whitelam, D. Joester, H. Zhang, J. D. Rimer, A. Navrotsky, J. F. Banfield, A. F. Wallace, F. M. Michel, F. C. Meldrum, H. Cölfen, P. M. Dove, *Science* **2015**, *349*, 6760.
- [6] J. Zhang, Y. Li, X. Zhang, B. Yang, *Adv. Mater.* **2010**, *22*, 4249.
- [7] S. Ni, L. Isa, H. Wolf, *Soft Matter* **2018**, *14*, 2978.
- [8] N. Vogel, M. Retsch, C. A. Fustin, A. Del Campo, U. Jonas, *Chem. Rev.* **2015**, *115*, 6265.
- [9] S. Sacanna, M. Korpics, K. Rodriguez, L. Colón-Meléndez, S.-H. Kim, D. J. Pine, G.-R. Yi, *Nat. Commun.* **2013**, *4*, 1688.
- [10] M. V. Kovalenko, L. Manna, A. Cabot, Z. Hens, D. V. Talapin, C. R. Kagan, V. I. Klimov, A. L. Rogach, P. Reiss, D. J. Milliron, P. Guyot-Sionnest, G. Konstantatos, W. J. Parak, T. Hyeon, B. A. Korgel, C. B. Murray, W. Heiss, *ACS Nano* **2015**, *9*, 1012.
- [11] E. Bianchi, R. Blaak, C. N. Likos, *Phys. Chem. Chem. Phys.* **2011**, *13*, 6397.
- [12] K. R. Phillips, G. T. England, S. Sunny, E. Shirman, T. Shirman, N. Vogel, J. Aizenberg, *Chem. Soc. Rev.* **2016**, *45*, 281.
- [13] B. Sciacca, A. Berkhout, B. J. M. Brenny, S. Z. Oener, M. A. van Huis, A. Polman, E. C. Garnett, *Adv. Mater.* **2017**, *29*, 1701064.
- [14] P. K. Kundu, D. Samanta, R. Leizrowice, B. Margulis, H. Zhao, M. Börner, T. Udayabhaskararao, D. Manna, R. Klajn, *Nat. Chem.* **2015**, *7*, 646.
- [15] K. J. Dorsey, T. G. Pearson, E. Esposito, S. Russell, B. Bircan, Y. Han, M. Z. Miskin, D. A. Muller, I. Cohen, P. L. McEuen, *Adv. Mater.* **2019**, *31*, 1901944.
- [16] M. J. Smith, C. H. Lin, S. Yu, V. V. Tsukruk, *Adv. Opt. Mater.* **2019**, *7*, 1801072.
- [17] B. C. Steimle, J. L. Fenton, R. E. Schaak, *Science* **2020**, *367*, 418.
- [18] B. J. Beberwyck, Y. Surendranath, A. P. Alivisatos, *J. Phys. Chem. C* **2013**, *117*, 19759.
- [19] L. De Trizio, L. Manna, *Chem. Rev.* **2016**, *116*, 10852.
- [20] J. M. Hodges, K. Kletetschka, J. L. Fenton, C. G. Read, R. E. Schaak, *Angew. Chem., Int. Ed.* **2015**, *54*, 8669.
- [21] T. Holtus, L. Helmbrecht, H. C. Hendrikse, I. Baglai, S. Meuret, G. W. P. Adhyaksa, E. C. Garnett, W. L. Noorduin, *Nat. Chem.* **2018**, *10*, 740.
- [22] A. E. Powell, J. M. Hodges, R. E. Schaak, *J. Am. Chem. Soc.* **2016**, *138*, 471.
- [23] C. D. Dieleman, W. Ding, L. Wu, N. Thakur, I. Bepalov, B. Daiber, Y. Ekinici, S. Castellanos, B. Ehrler, *Nanoscale* **2020**, *12*, 11306.
- [24] K. Miszta, F. Greullet, S. Marras, M. Prato, A. Toma, M. Arciniegas, L. Manna, R. Krahne, *Nano Lett.* **2014**, *14*, 2116.
- [25] R. J. Jackman, J. L. Wilbur, G. M. Whitesides, *Science* **1995**, *269*, 664.
- [26] T. Kraus, L. Malaquin, H. Schmid, W. Riess, N. D. Spencer, H. Wolf, *Nat. Nanotechnol.* **2007**, *2*, 570.
- [27] A. Perl, D. N. Reinhoudt, J. Huskens, *Adv. Mater.* **2009**, *21*, 2257.
- [28] R. Klajn, M. Fialkowski, I. T. Bensemann, A. Bitner, C. J. Campbell, K. Bishop, S. Smoukov, B. A. Grzybowski, *Nat. Mater.* **2004**, *3*, 729.
- [29] Q. A. Akkerman, G. Rainò, M. V. Kovalenko, L. Manna, *Nat. Mater.* **2018**, *17*, 394.
- [30] S. D. Stranks, H. J. Snaith, *Nat. Nanotechnol.* **2015**, *10*, 391.
- [31] M. A. Green, A. Ho-Baillie, *ACS Energy Lett.* **2017**, *2*, 822.
- [32] W. Lee, J. Lee, H. Yun, J. Kim, J. Park, C. Choi, D. C. Kim, H. Seo, H. Lee, J. W. Yu, W. B. Lee, D. H. Kim, *Adv. Mater.* **2017**, *29*, 1702902.

- [33] F. Zhang, H. Zhong, C. Chen, X. G. Wu, X. Hu, H. Huang, J. Han, B. Zou, Y. Dong, *ACS Nano* **2015**, *9*, 4533.
- [34] J. Xue, Z. Zhu, X. Xu, Y. Gu, S. Wang, L. Xu, Y. Zou, J. Song, H. Zeng, Q. Chen, *Nano Lett.* **2018**, *18*, 7628.
- [35] Y. Wei, Z. Cheng, J. Lin, *Chem. Soc. Rev.* **2019**, *48*, 310.
- [36] H. Wei, Y. Fang, P. Mulligan, W. Chuirazzi, H. H. Fang, C. Wang, B. R. Ecker, Y. Gao, M. A. Loi, L. Cao, J. Huang, *Nat. Photonics* **2016**, *10*, 333.
- [37] Q. Chen, J. Wu, X. Ou, B. Huang, J. Almutlaq, A. A. Zhumekenov, X. Guan, S. Han, L. Liang, Z. Yi, J. Li, X. Xie, Y. Wang, Y. Li, D. Fan, D. B. L. Teh, A. H. All, O. F. Mohammed, O. M. Bakr, T. Wu, M. Bettinelli, H. Yang, W. Huang, X. Liu, *Nature* **2018**, *561*, 88.
- [38] C. H. Lin, Q. Zeng, E. Lafalce, S. Yu, M. J. Smith, Y. J. Yoon, Y. Chang, Y. Jiang, Z. Lin, Z. V. Vardeny, V. V. Tsukruk, *Adv. Opt. Mater.* **2018**, *6*, 1800474.
- [39] C.-K. Lin, Q. Zhao, Y. Zhang, S. Cestellos-Blanco, Q. Kong, M. Lai, J. Kang, P. Yang, *ACS Nano* **2020**, *14*, 3500.
- [40] M. E. Kamminga, H. H. Fang, M. A. Loi, G. H. Ten Brink, G. R. Blake, T. T. M. Palstra, J. E. Ten Elshof, *ACS Appl. Mater. Interfaces* **2018**, *10*, 12878.
- [41] G. Wang, D. Li, H. C. Cheng, Y. Li, C. Y. Chen, A. Yin, Z. Zhao, Z. Lin, H. Wu, Q. He, M. Ding, Y. Liu, Y. Huang, X. Duan, *Sci. Adv.* **2015**, *1*, 1500613.
- [42] B. H. Kim, M. S. Onses, J. Bin Lim, S. Nam, N. Oh, H. Kim, K. J. Yu, J. W. Lee, J. H. Kim, S. K. Kang, C. H. Lee, J. Lee, J. H. Shin, N. H. Kim, C. Leal, M. Shim, J. A. Rogers, *Nano Lett.* **2015**, *15*, 969.
- [43] J. Chen, Y. Wu, X. Li, F. Cao, Y. Gu, K. Liu, X. Liu, Y. Dong, J. Ji, H. Zeng, *Adv. Mater. Technol.* **2017**, *2*, 1700132.
- [44] C. Zhang, B. Wang, W. Li, S. Huang, L. Kong, Z. Li, L. Li, *Nat. Commun.* **2017**, *8*, 1138.
- [45] H. Wang, R. Haroldson, B. Balachandran, A. Zakhidov, S. Sohal, J. Y. Chan, A. Zakhidov, W. Hu, *ACS Nano* **2016**, *10*, 10921.
- [46] N. Pourdavoud, S. Wang, A. Mayer, T. Hu, Y. Chen, A. Marianovich, W. Kowalsky, R. Heiderhoff, H.-C. Scheer, T. Riedl, *Adv. Mater.* **2017**, *29*, 1605003.
- [47] O. Bar-On, P. Brenner, U. Lemmer, J. Scheuer, *Adv. Mater. Technol.* **2018**, *3*, 1800212.
- [48] F. Palazon, Q. A. Akkerman, M. Prato, L. Manna, *ACS Nano* **2016**, *10*, 1224.
- [49] Y. C. Wong, W. Bin Wu, T. Wang, J. D. A. Ng, K. H. Khoo, J. Wu, Z. K. Tan, *Adv. Mater.* **2019**, *31*, 1901185.
- [50] H. L. Clever, F. J. Johnston, *J. Phys. Chem. Ref. Data* **1980**, *9*, 751.
- [51] A. A. Zhumekenov, M. I. Saidaminov, M. A. Haque, E. Alarousu, S. P. Sarmah, B. Murali, I. Dursun, X. H. Miao, A. L. Abdelhady, T. Wu, O. F. Mohammed, O. M. Bakr, *ACS Energy Lett.* **2016**, *1*, 32.
- [52] L. Hong, J. Milic, P. Ahlwat, M. Mladenovic, D. J. Kubicki, F. Jahanbakhshi, D. Ren, M. Gelvez-Rueda, M. A. Ruiz-Preciado, A. Ummadisingu, Y. Liu, C. Tian, L. Pan, S. M. Zakeeruddin, A. Hagfeldt, F. C. Grozema, U. Rothlisberger, L. Emsley, H. Han, M. Grätzel, *Angew. Chem., Int. Ed.* **2020**, *59*, 4691.
- [53] Y. T. H. Kim, G. H. Lee, Y. T. H. Kim, C. Wolf, H. J. Yun, W. Kwon, C. G. Park, T. W. Lee, *Nano Energy* **2017**, *38*, 51.
- [54] H. Fang, W. Deng, X. Zhang, X. Xu, M. Zhang, J. Jie, X. Zhang, *Nano Res.* **2019**, *12*, 171.
- [55] C. Cennini, G. Tambroni, *Di Cennino Cennini Trattato Della Pittura*, Paolo Salviucci, Rome **1821**.
- [56] W. Anaf, O. Schalm, K. Janssens, K. De Wael, *Dyes Pigm.* **2015**, *113*, 409.
- [57] V. Rahemi, N. Sarmadian, W. Anaf, K. Janssens, D. Lamoen, B. Partoens, K. De Wael, *Anal. Chem.* **2017**, *89*, 3326.
- [58] I. Fiedler, M. Bayard, in *Artists' Pigments: A Handbook of Their History and Characteristics* (Ed: R. L. Feller), National Gallery of Art, Washington, in association with Archetype Publications Ltd., London **1986**, p. 104.
- [59] M. Eder, S. Amini, P. Fratzl, *Science* **2018**, *362*, 543.
- [60] M. R. Begley, D. S. Gianola, T. R. Ray, *Science* **2019**, 364.
- [61] F. L. Bargardi, H. L. Ferrand, R. Libanori, A. R. Studart, *Nat. Commun.* **2016**, *7*, 13912.
- [62] Portrait of Marie Skłodowska Curie (1867–1934), Polish-French physicist and chemist, Nobel Laureate in physics (1903) and chemistry (1911) (Wellcome Collection), <https://wellcomecollection.org/works/s7fye3z3> (accessed: September 2020).